Supplementary Information (SI) for Nanoscale Horizons.
This journal is © The Royal Society of Chemistry 2026

Supporting information

Growing Bright: Ligand-Controlled Growth of Aqueous Colloidal Cu-In-Zn-S Nanocrystals

Caterina Bellatreccia,[a] Angelica Germinario,[a] Zakaria Ziani,[a†] Alessandro Gradone,[b] Sirous Khabbaz Abkenar,[c] Giorgio Divitini,[c] Marco Villa,[a*] and Paola Ceroni[a*]

[a] Dipartimento di Chimica "Giacomo Ciamician" Alma Mater Studiorum – Università di Bologna Via Selmi 2, Bologna 40126, Italy

[b] Istituto per lo Studio dei Materiali Nanostrutturati (ISMN) - CNR Sede di Bologna, via Gobetti 101, Bologna 40129, Italy

[c] Electron Spectroscopy and Nanoscopy, Istituto Italiano di Tecnologia, via Morego 30, Genoa *16163, Italy*

[†] *Current address: Université Paris Cité, CNRS, ITODYS, F-75013 Paris, France*

Contents

Synthesis and structural characterisation of CIZS@L1-L2

Synthesis with non-thiolated ligands: The same procedure described in the experimental section for synthesis of **CIZS@L1-L2** is employed with **L1** = **CIT** and **L2** = alanine (**ALA**), lysine (**LYS**), tyrosine (**TYR**) and phenylalanine (**Ph-ALA**). All these batches show very limited colloidal stability: all of them except **CIZS@CIT-ALA** precipitate during the synthesis and cannot be recovered nor analysed. **CIZS@CIT-ALA** shows limited precipitation and therefore could be analysed right after synthesis (Figure S1). Its absorption and emission spectrum shows that CIZS can be obtained even with non-thiolated ligands, but in this case the PLQY is drastically lower (<2%) even right after synthesis. In addition to that, **CIZS@CIT-ALA** completely precipitates within 2 days. Therefore, non-thiolated ligands are certainly less-suitable than thiolated ligands in this water-based synthesis.

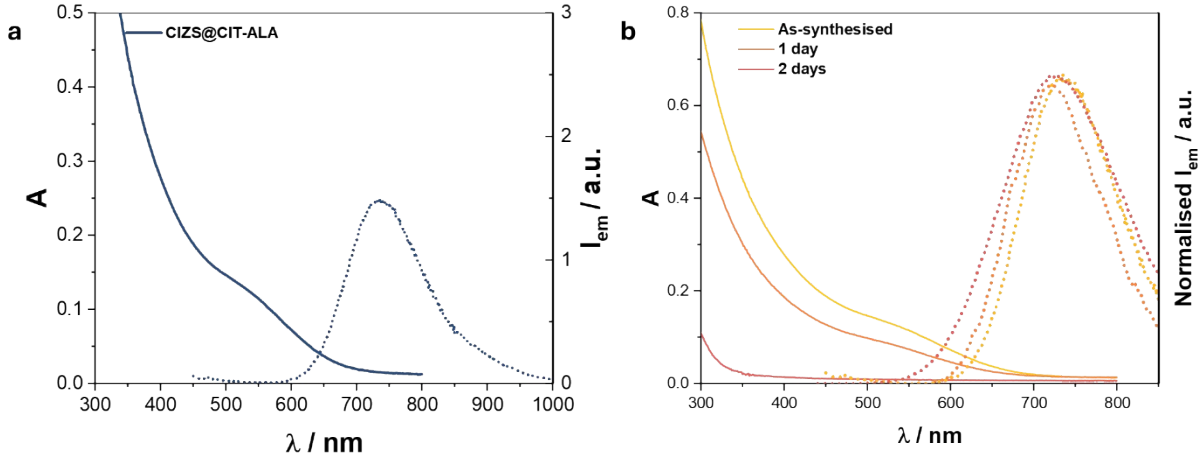

Figure S1. a) Absorption (solid line) and emission spectra (dotted line) of **CIZS@CIT-ALA** in air-equilibrated aqueous solution. b) Time-evolution of the photophysical properties of **CIZS@CIT-** upon storage at room temperature in air-equilibrated aqueous solution. For emission spectra, λ_{exc} = 350 nm.

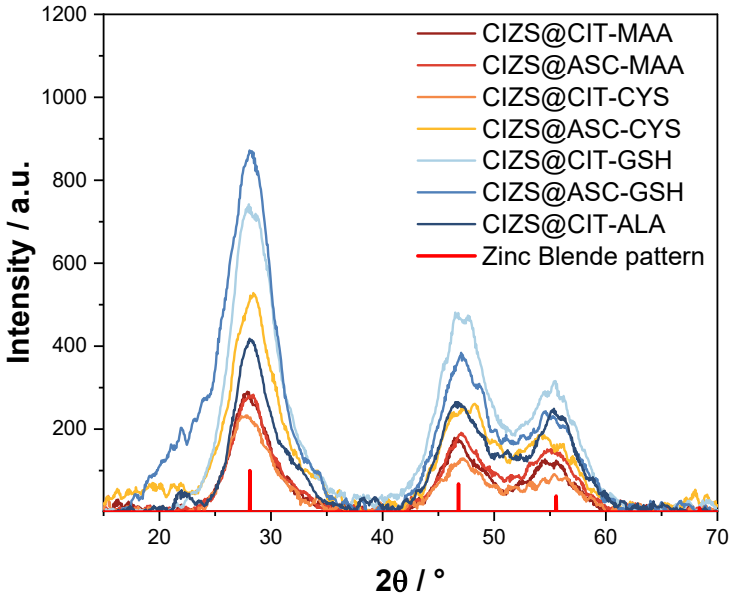

Figure S2. XRD pattern of **CIZS@L1-L2**. The samples are precipitated in acetone and dried under vacuum to obtain a powder. The XRD is acquired with a zero-background silicon sample holder. Calculated spectra of zinc blende $CuInS_2$ (red bottom line) are reported for comparison.

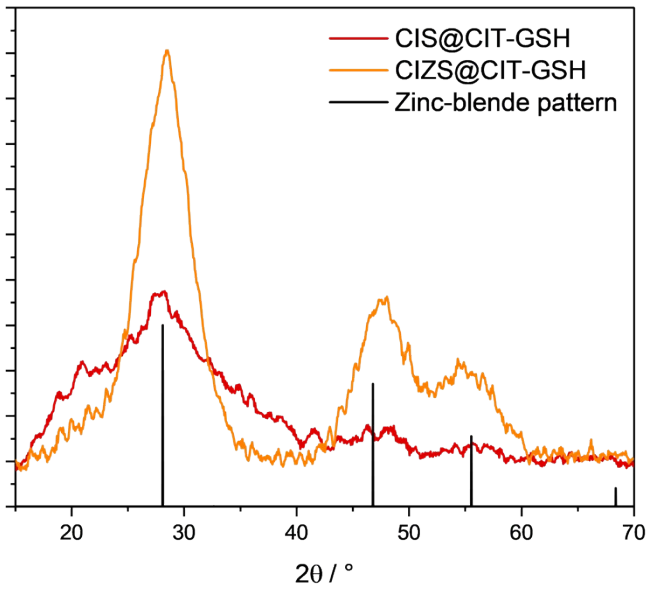

Figure S3. Comparison of the XRD pattern of **CIZS@CIT-GSH** and **CIS@CIT-GSH**. The samples are precipitated in acetone and dried under vacuum to obtain a powder. The XRD is acquired with a zero-background silicon sample holder. Calculated spectra of zinc blende $CuInS_2$ (red bottom line) are reported for comparison.

The comparison between a representative sample before (**CIS@CIT-GSH**) and after the addition of the Zn-shell precursor solution (**CIZS@CIT-GSH**) shows that even the core-only

nanocrystals display zinc-blende structure. Nevertheless, the diffraction peaks are broader and less intense, suggesting a smaller crystallite dimension or a lower crystallinity within the nanoparticle.

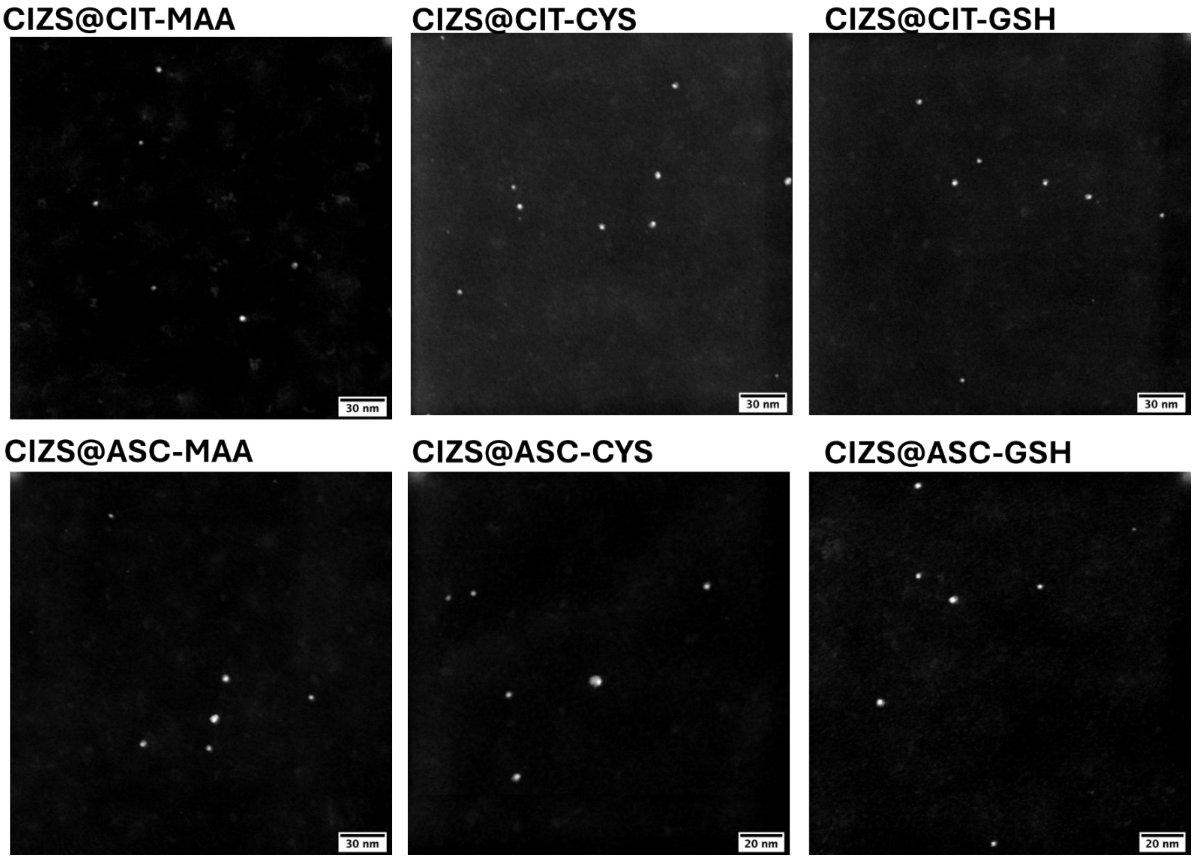

Figure S4. HAADF-STEM images of **CIZS@L1-L2**. These images were used for statistical size analysis measuring the area of each particle.

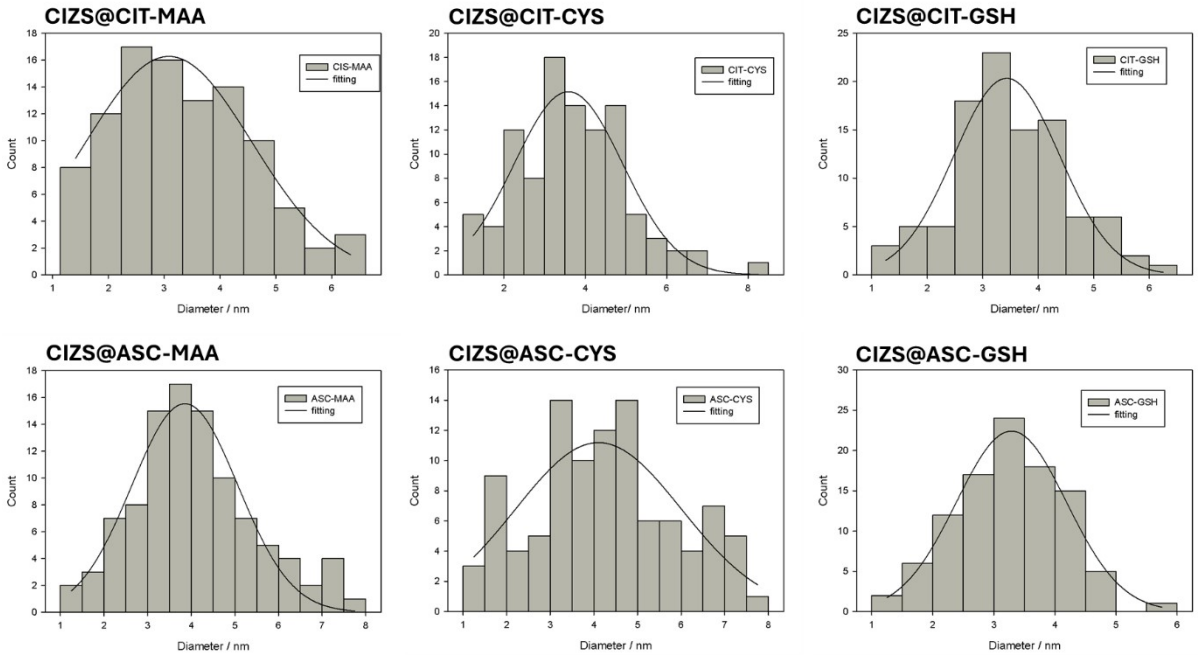

Figure S5. Size distribution histograms for each sample. In total around 100 nanoparticles per sample have been evaluated, considering the ones with spherical morphology. All fittings are made using a gaussian equation (3 parameters): $y = a\, e^{[-0.5*(x-x_0)/2]}$.

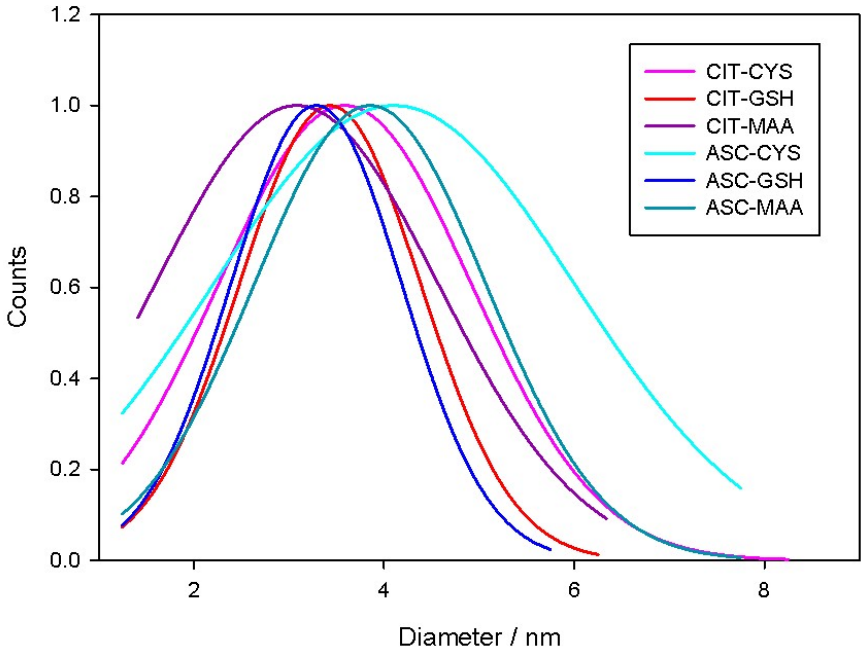

Figure S6. Size distribution fitting curves of **CIZS@L1-L2**.

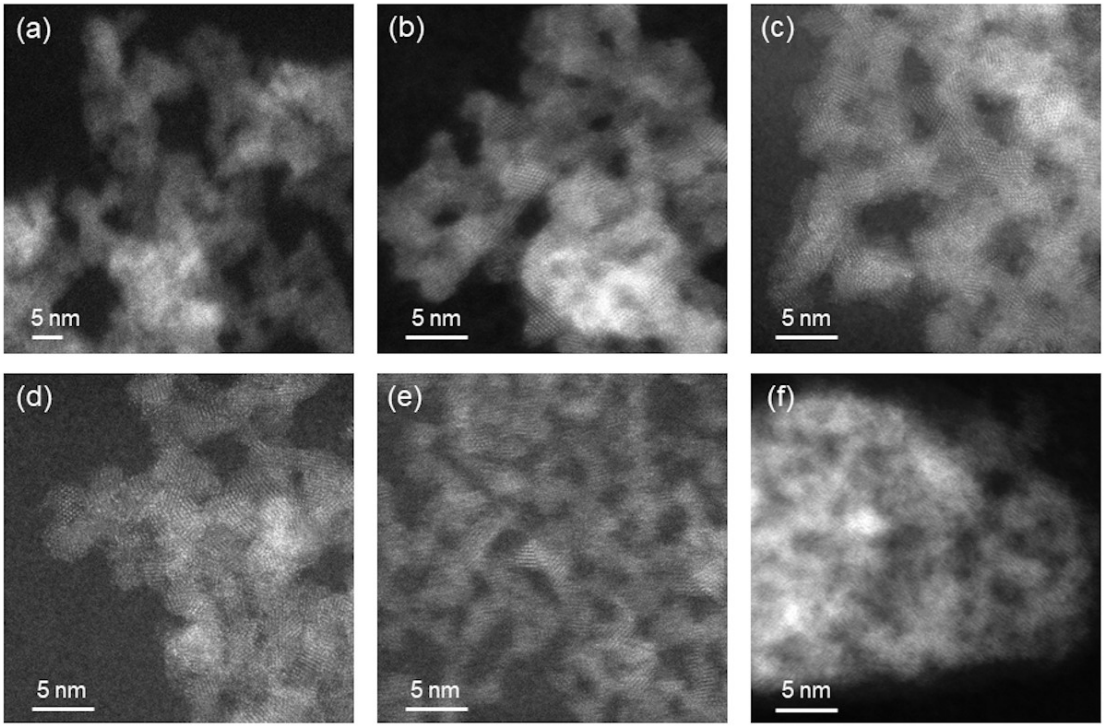

Figure S7. Representative HAADF-HRSTEM images of the different CIZS and CIS nanocrystal samples. (a) **CIZS@CIT-MAA**, (b) **CIZS@ASC-MAA**, (c) **CIZS@CIT-CYS**, (d) **CIZS@ASC-CYS**, (e) **CIZS@CIT-GSH** and (f) **CIS@CIT-GSH**.

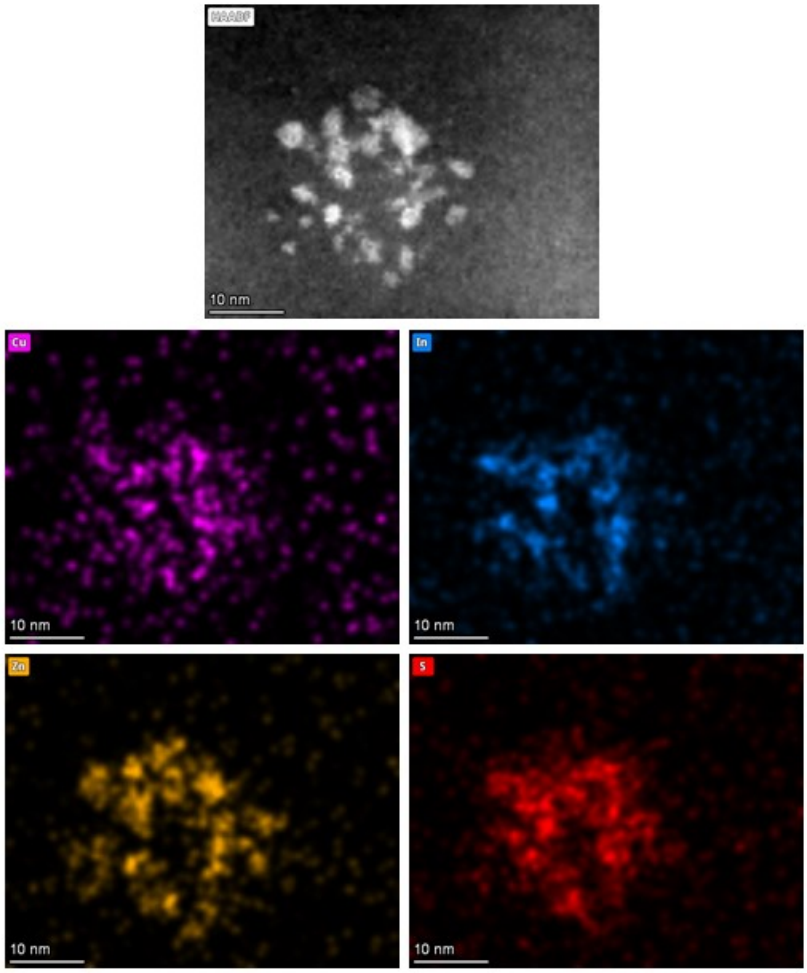

Figure S8. HAADF-STEM image and corresponding EDX elemental maps of the **CIZS@CIT-GSH** quantum dots. The HAADF micrograph (top) shows a cluster of nanocrystals, while the elemental maps (bottom) reveal the spatial distribution of Cu, In, Zn and S within the aggregate.

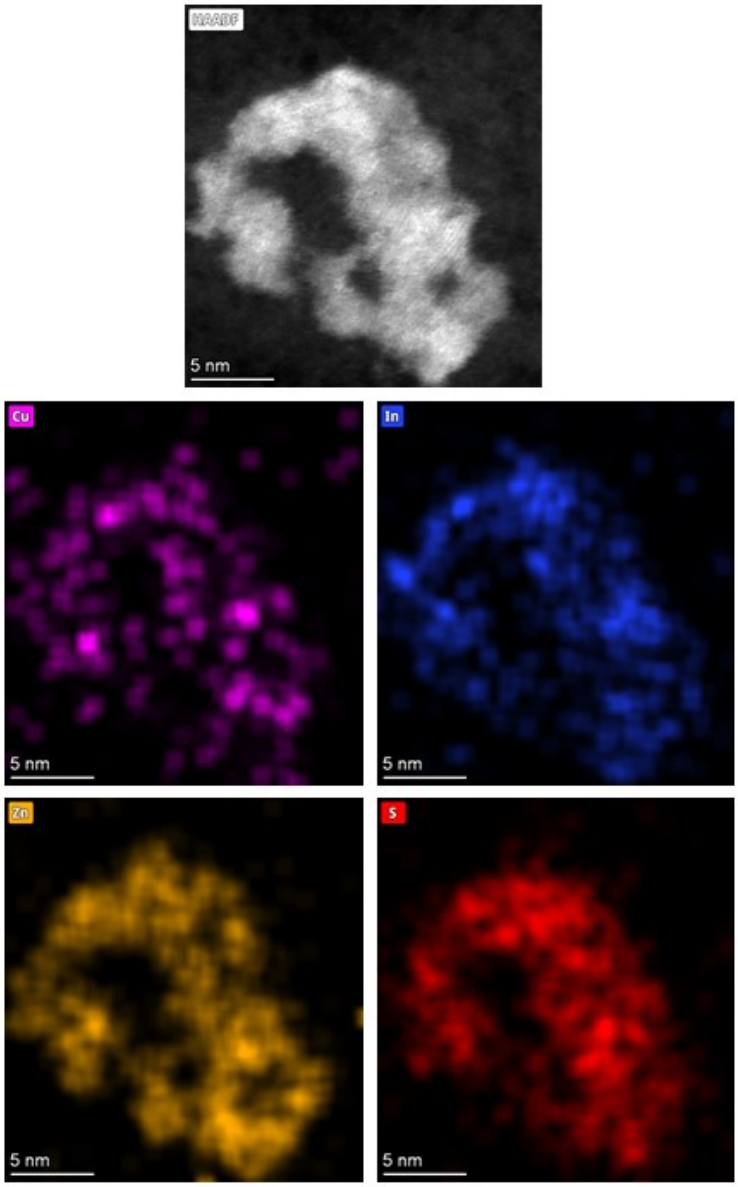

Figure S9. HAADF-STEM image and corresponding EDX elemental maps of the **CIZS@ASC-MAA** quantum dots. The HAADF micrograph (top) displays the aggregated nanocrystal network, while the elemental maps (bottom) show the distributions of Cu, In, Zn and S across the structure.

EDX mapping of both **CIZS@ASC-MAA** and **CIZS@CIT-GSH** reveal that Cu and In are predominantly localized in the central regions of the aggregated particles, whereas Zn is distributed more uniformly over the entire particle volume. This distribution pattern supports an alloyed structural model with graded composition, in which the nanoparticles possess Cu/In-rich cores and Zn-rich outer layers.

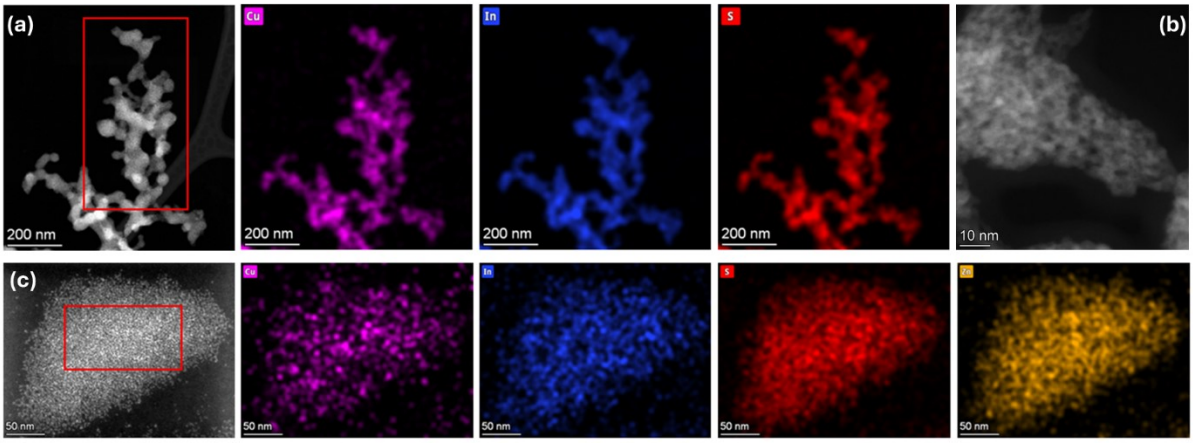

Figure S10. STEM-EDX comparison of the **CIS** and the final **CIZS** specimens obtained with **CIT–GSH** ligands: a) HAADF-STEM image of the **CIS@CIT-GSH** aliquot collected prior to Zn addition, together with the corresponding elemental maps for Cu, In and S. b) Enlarged HAADF-STEM image of the **CIS@CIT-GSH** aliquot collected prior to Zn addition. c) HAADF-STEM image of the CISZ@CIT-GSH sample collected after Zn addition, shown with the elemental maps for Cu, In, Zn and S.

In each case, the red box indicates the region integrated for quantitative EDX analysis. The accompanying table summarizes the atomic fractions measured in the selected regions, highlighting the marked decrease in Cu and the incorporation of Zn in the final CIZS product.

Table S1: Quantitative STEM-EDX composition extracted from the boxed regions in the **CIS@CIT-GSH** (before Zn addition) and **CIZS@CIT-GSH** (after Zn addition) samples.

Sample ID	Atomic Fraction (%)				
	In	O	Cu	S	Zn
CIS@CIT-GSH	20.9 ± 2.1	46.0 ± 2.5	8.5 ± 1.2	24.6 ± 3.5	-
CISZ@CIT-GSH	3.7 ± 0.5	41.8 ± 3.1	1.9 ± 0.3	33.7 ± 4.3	18.9 ± 2.4

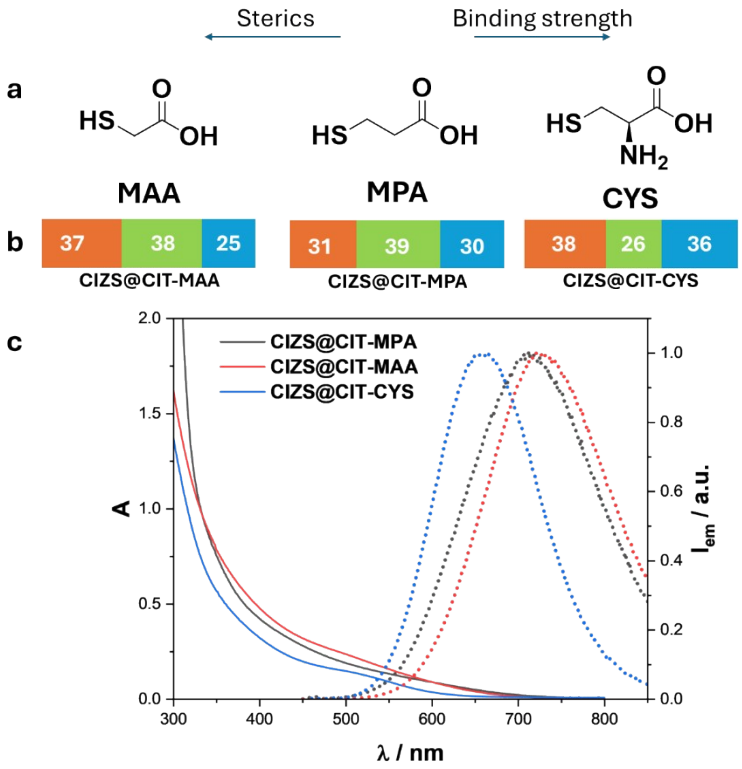

Figure S11. a) Structure of the soft ligands **CYS**, **MPA** and **MAA**; b) Chemical composition of **CIZS@CIT-L2** as detected by MP-AES; c) Absorption (solid line) and emission spectra (dashed line) of **CIZS@CIT-L2**, where L2 are **CYS**, **MPA** or **MAA**.

Additional photophysical data

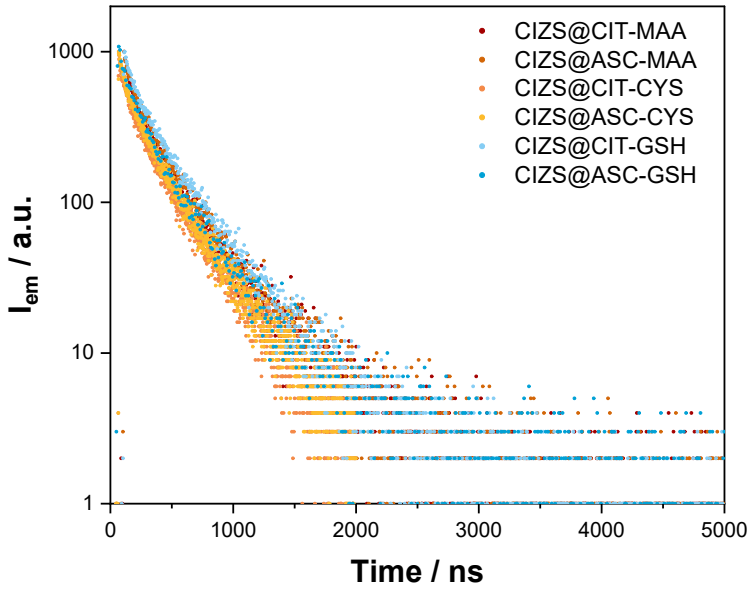

Figure S12. Emission decays of **CIZS@L1-L2** samples. λ_{exc}: 405 nm; λ_{em}: 640 nm.

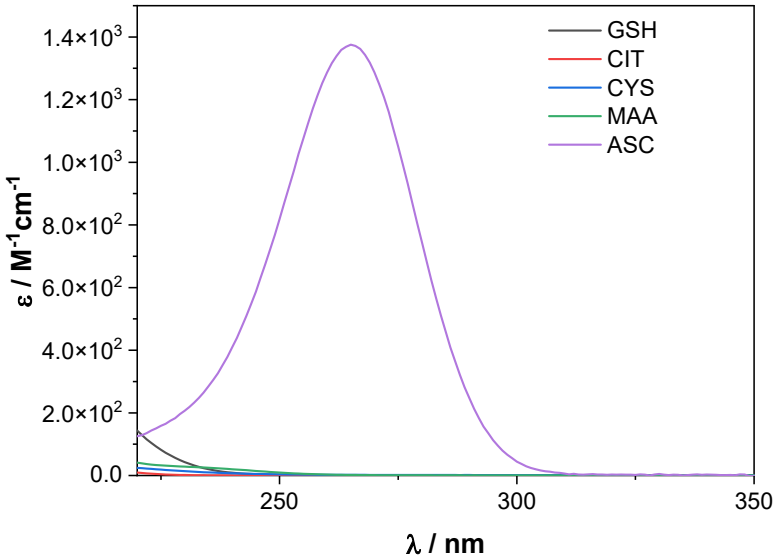

Figure S13. Absorption spectra of **L1** and **L2** ligands in air-equilibrated aqueous solution.

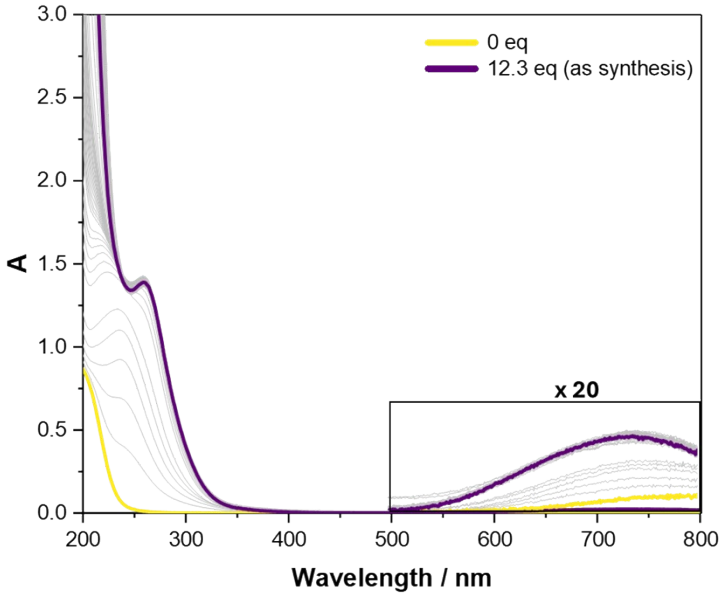

Figure S14. Spectrophotometric titration of a solution of $CuCl_2$ (0.6 mM) with **NaCIT** (40 mM) in air-equilibrated aqueous solution.

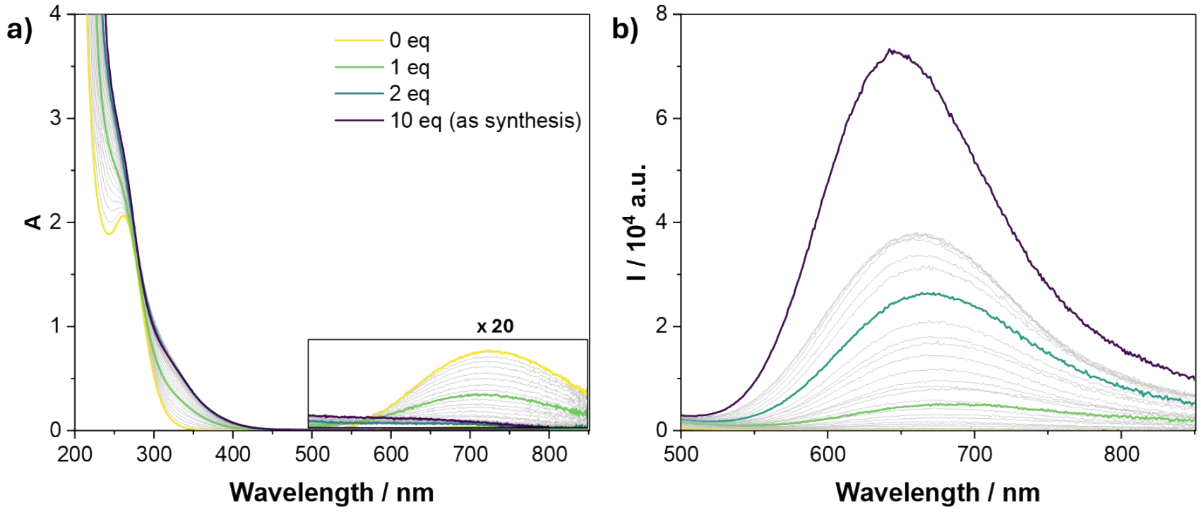

Figure S15. a) Spectrophotometric titration of the mixture $CuCl_2$ (0.6 mM) + $InCl_3$ (2.0 mM) + **CIT** (7.4 mM) with **GSH** (6 mM) in aqueous solution and b) emission spectra of the same solution (λ_{exc} = 350 nm). After addition of **CIT**, the solution was deaerated *via* Ar-bubbling. In presence of O_2, the nanoclusters that are formed during the titration are not stable due to oxidation of Cu^+ to Cu^{2+} by O_2, and the changes observed on the band at 715 nm are not stable over time.

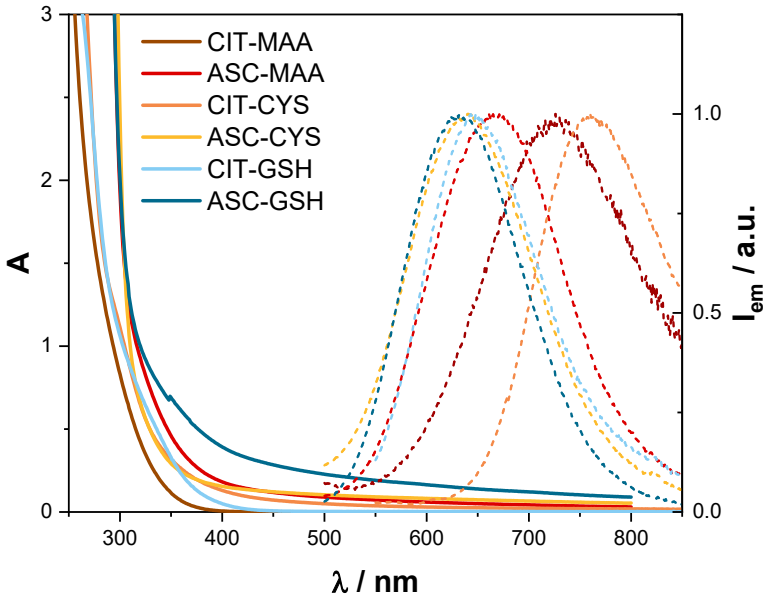

Figure S16. Absorption (solid line) and emission (dotted line) of the mixture $CuCl_2$ (0.6 mM) + $InCl_3$ (2 mM) + **L1** (7.5 mM) + **L2** (12 mM). The spectra are indicated with the **L1-L2** couple used for that sample. Samples with ascorbate show lower solubility, as highlighted by the high baseline at 800 nm due to light scattering.

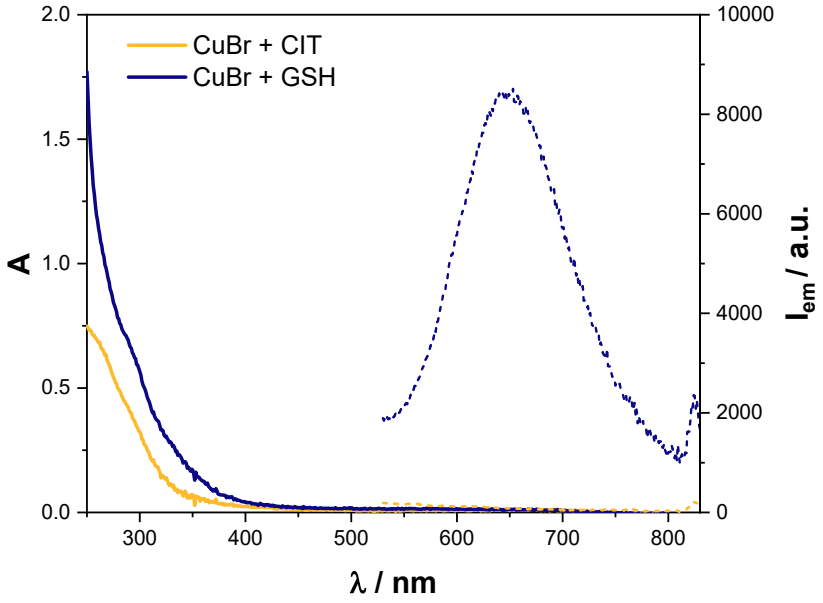

Figure S17: Absorption (solid lines) and emission (dashed line) of acqueous solutions of CuBr + CIT (yellow line) and CuBr + GSH (blue line). The same molar ratio as in Figure S10 have been employed.

Growth kinetics of CIZS@L1-L2

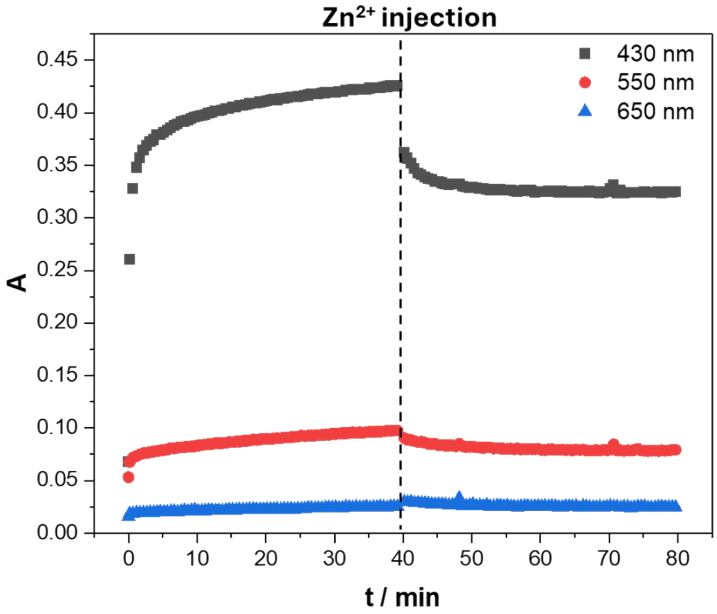

Figure S18: Kinetic evolution of the absorption value at different wavelengths of **CIZS@CIT-GSH** during air-equilibrated synthesis at 70°C.

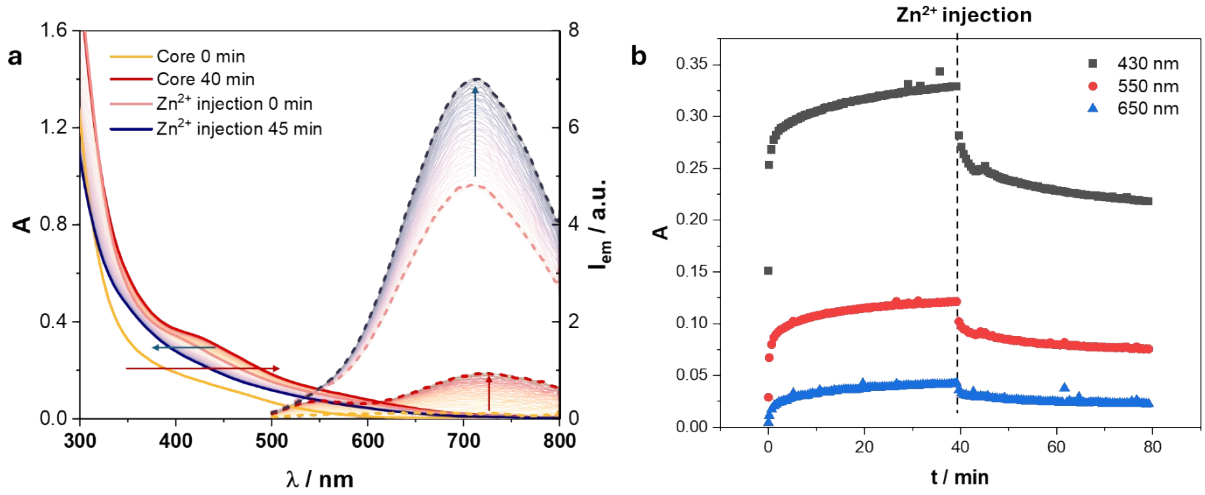

Figure S19: a) Kinetic evolution of absorption (solid lines) and emission (dotted lines) of **CIZS@CIT-MAA** during air-equilibrated synthesis at 70°C. b) Kinetic evolution of the absorption value at different wavelengths of **CIZS@CIT-MAA** during air-equilibrated synthesis at 70°C.

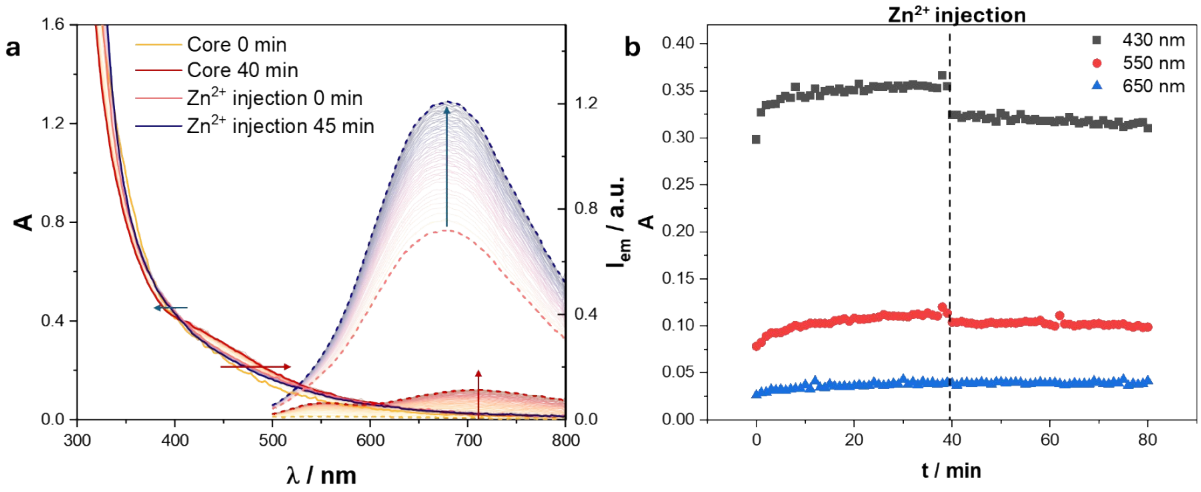

Figure S20: a) Kinetic evolution of absorption (solid lines) and emission (dotted lines) of **CIZS@ASC-MAA** during air-equilibrated synthesis at 70°C. b) Kinetic evolution of the absorption value at different wavelengths of **CIZS@ASC-MAA** during air-equilibrated synthesis at 70°C.

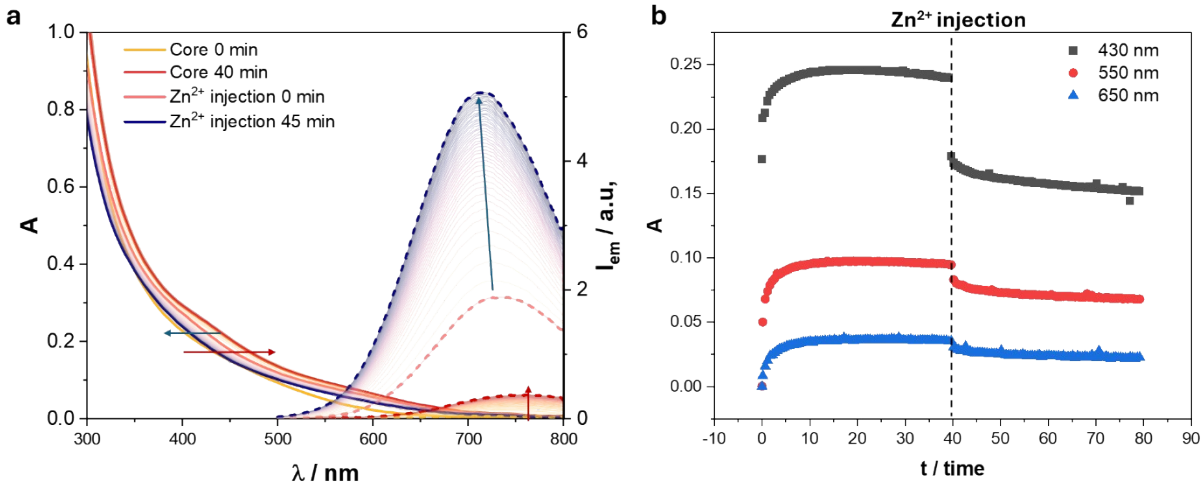

Figure S21: a) Kinetic evolution of absorption (solid lines) and emission (dotted lines) of **CIZS@CIT-CYS** during air-equilibrated synthesis at 70°C. b) Kinetic evolution of the absorption value at different wavelengths of **CIZS@CIT-CYS** during air-equilibrated synthesis at 70°C.

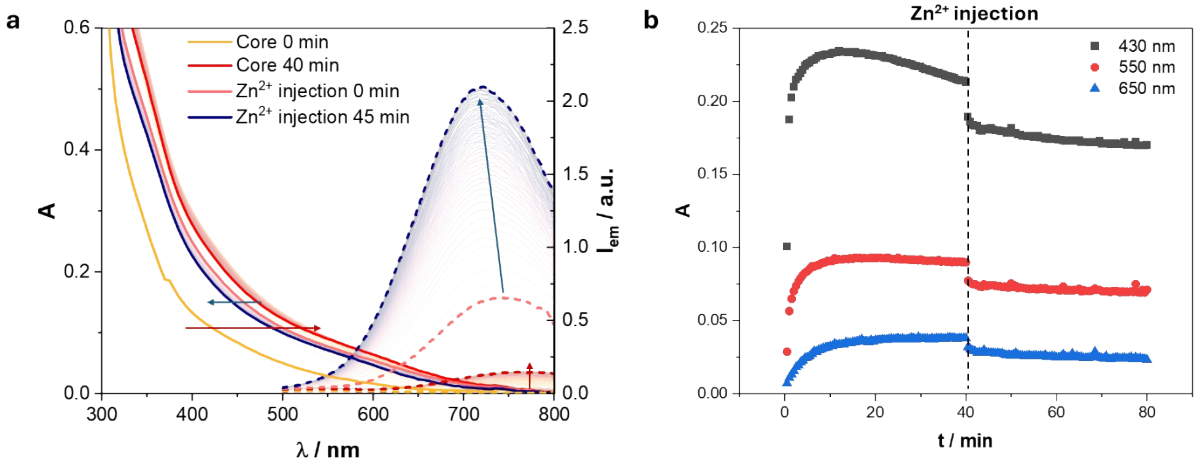

Figure S22: a) Kinetic evolution of absorption (solid lines) and emission (dotted lines) of **CIZS@ASC-CYS** during air-equilibrated synthesis at 70°C. b) Kinetic evolution of the absorption value at different wavelengths of **CIZS@ASC-CYS** during air-equilibrated synthesis at 70°C.

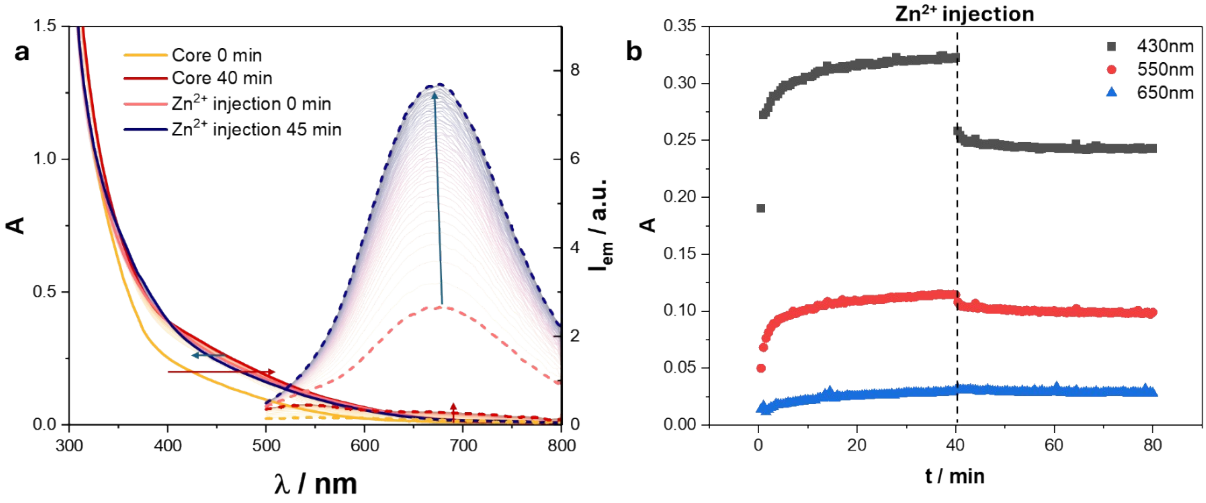

Figure S23: a) Kinetic evolution of absorption (solid lines) and emission (dotted lines) of **CIZS@ASC-GSH** during air-equilibrated synthesis at 70°C. b) Kinetic evolution of the absorption value at different wavelengths of **CIZS@ASC-GSH** during air-equilibrated synthesis at 70°C.

The kinetic evolutions of **CIZS-CITCYS** and **CIZS-ASCCYS** show a slight decrease of the absorption at 430 nm after 20 minutes of core growth. This may indicate that the corrosion of the CIS core by cysteine already starts during the core synthesis, facilitated by the high temperature and the absence of protecting ZnS layers. The speed of the reaction, observed even at lower temperatures, leads to limited control over the dimensions of the resulting nanocrystal, which essentially remains unchanged after the first 10 minutes of reaction for all the **L1-L2** couples.

Stability of CIZS@L1-L2

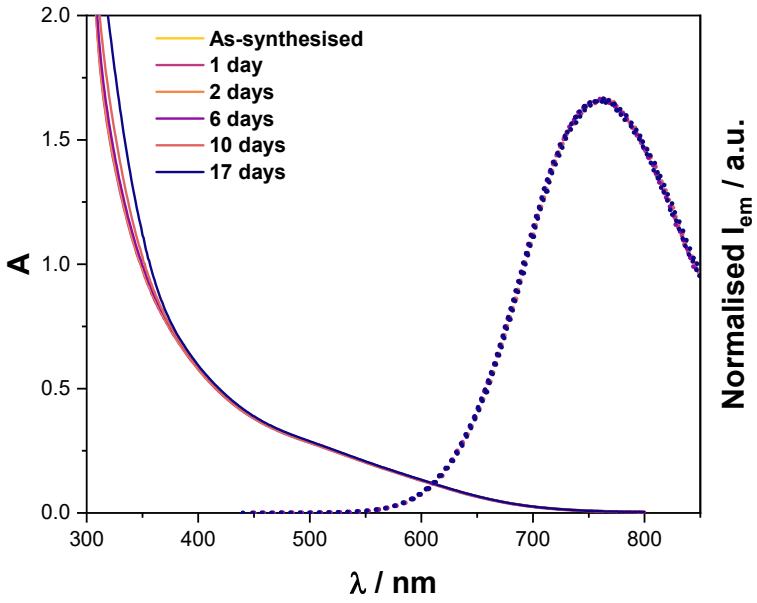

Figure S24: Evolution of absorption (solid line) and emission (dashed line) of **CIZS@CIT-MAA** over time. Batches were stored at room temperature under air-equilibrated conditions. For emission, λ_{exc} = 350 nm

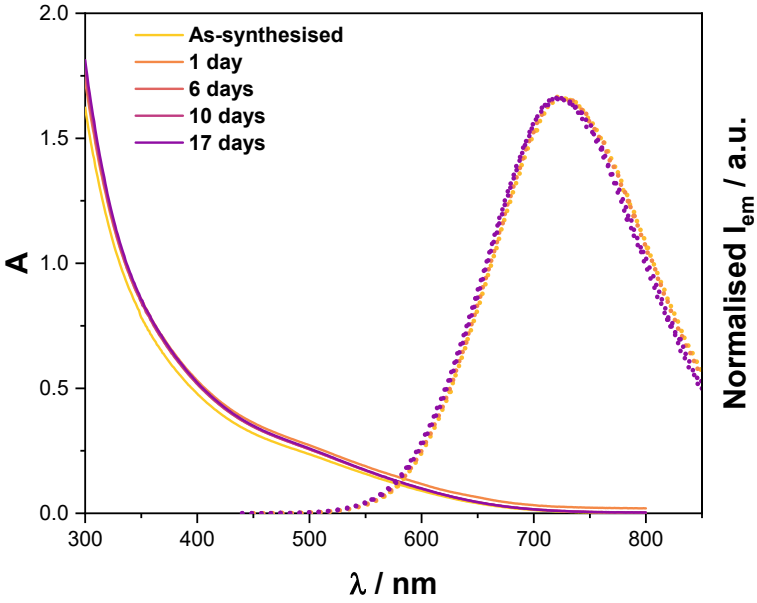

Figure S25: Evolution of absorption (solid line) and emission (dashed line) of **CIZS@ASC-MAA** over time. Batches were stored at room temperature under air-equilibrated conditions. For emission, λ_{exc} = 350 nm

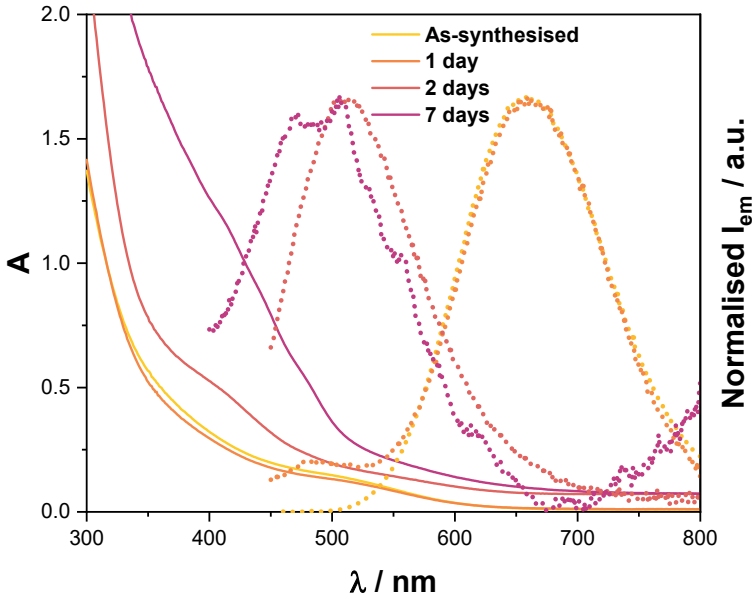

Figure 26: Evolution of absorption (solid line) and emission (dashed line) of **CIZS@CIT-CYS** over time. Batches were stored at room temperature under air-equilibrated conditions. For emission, λ_{exc} = 350 nm

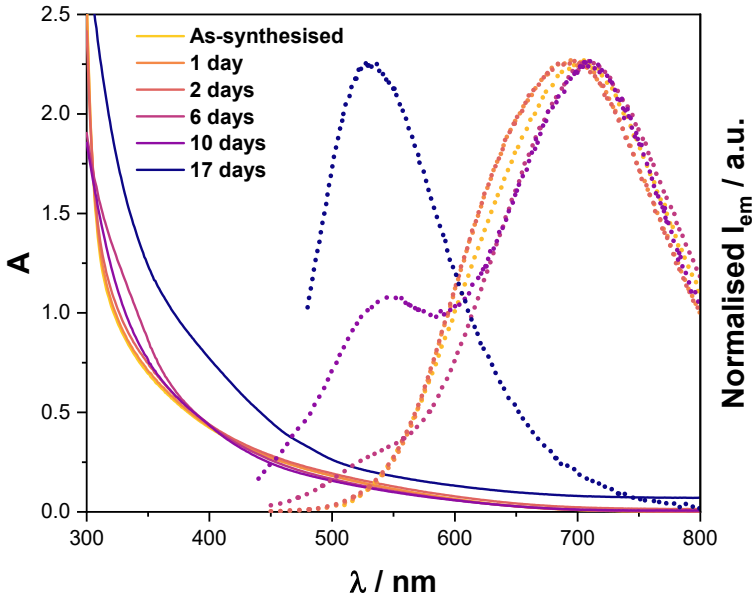

Figure S27: Evolution of absorption (solid line) and emission (dashed line) of **CIZS@ASC-CYS** over time. Batches were stored at room temperature under air-equilibrated conditions. For emission, λ_{exc} = 350 nm

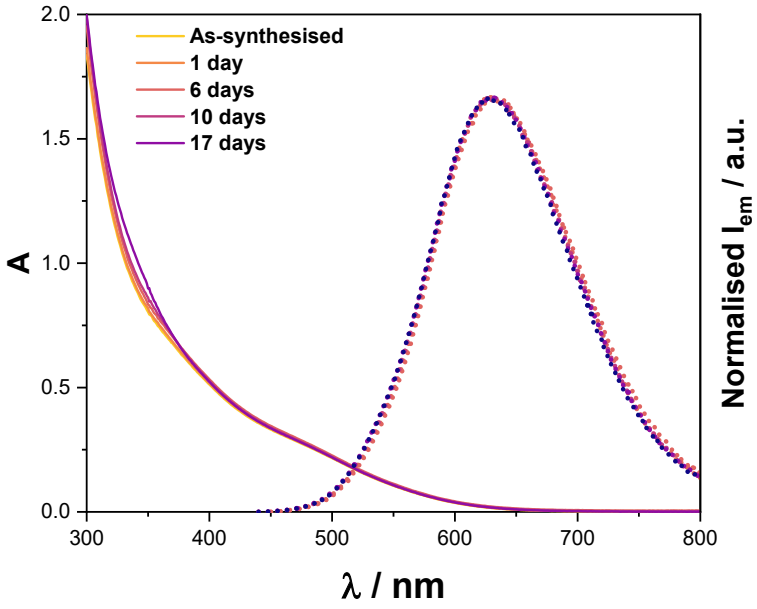

Figure S28: Evolution of absorption (solid line) and emission (dashed line) of **CIZS@CIT-GSH** over time. Batches were stored at room temperature under air-equilibrated conditions. For emission, λ_{exc} = 350 nm

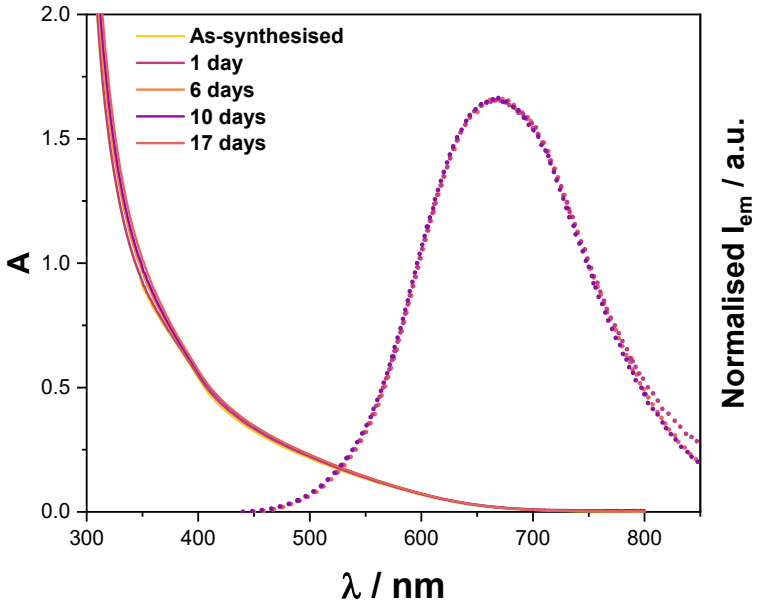

Figure S29: Evolution of absorption (solid line) and emission (dashed line) of **CIZS@ASC-GSH** over time. Batches were stored at room temperature under air-equilibrated conditions. For emission, λ_{exc} = 350 nm

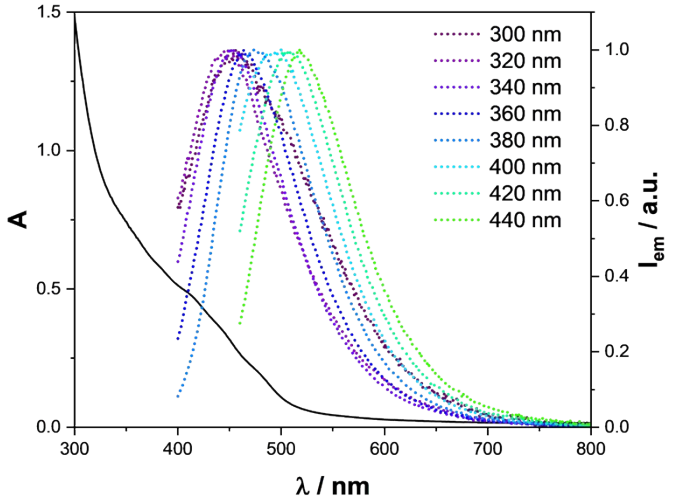

Figure S30: Absorption (solid line) and emission at varying exciting wavelength (dashed lines) of **CIZS@CIT-CYS** after 2 weeks in air-equilibrated aqueous solution. The legend indicates the exciting wavelength for each emission spectrum.

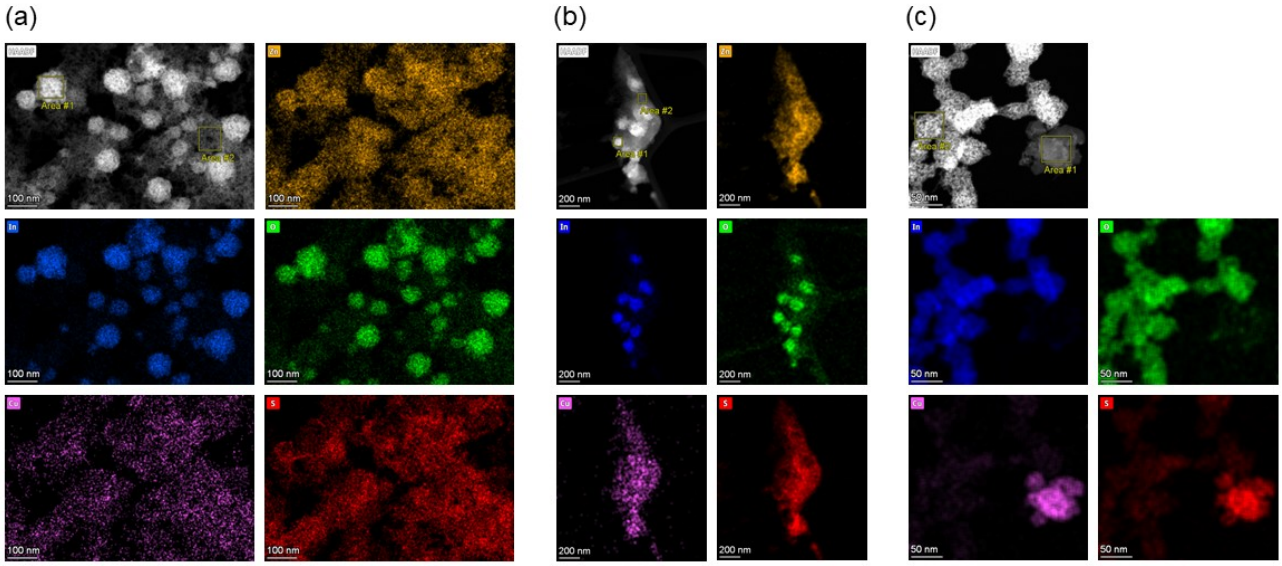

Figure S31: STEM-EDX analysis of ligand-capped Cu–In–Zn–S nanocrystals after 4 weeks of storage in aqueous solution. (a) **CIZS@CIT-CYS**, (b) **CIZS@ASC-MAA** and (c) **CIS@CIT-GSH**. For each sample, the HAADF-STEM image (left) is shown together with the corresponding EDX elemental maps for Zn, In, O, Cu and S. Yellow squares (Area #1 and Area #2) indicate the regions used for quantitative EDX analysis summarized in Table S2. A clear correlation between In and O and between Cu and S can be observed.

Table S2: Quantitative STEM-EDX analysis of selected regions of interest (ROIs) in **CIZS@CIT-CYS**, **CIZS@ASC-MAA** and **CIS@CIT-GSH** samples. Listed values are atomic fractions (at.%) of In, O, Cu, S and Zn averaged over the indicated ROIs (Area 1 and Area 2 in Figure S31).

Sample ID	ROI	Atomic Fraction (%)				
		In	O	Cu	S	Zn
CIZS@CIT-CYS	Area 1	16.1 ± 1.5	66.7 ± 1.7	0.5 ± 0.1	3.8 ± 0.6	12.9± 1.5
	Area 2	2.2 ± 0.3	26.6 ± 2.1	3.4 ± 0.5	35.7 ± 4.5	32.1 ± 3.6
CIZS@ASC-MAA	Area 1	17.2 ± 1.6	64.0 ± 1.8	1.4 ± 0.3	9.3 ± 1.6	8.1 ± 1.0
	Area 2	1.7 ± 0.3	18.3 ± 1.8	1.7 ± 0.4	43.4 ± 5.1	34.9 ± 4.2
CIS@CIT-GSH	Area 1	0.6 ± 0.1	13.0 ± 1.3	41.4 ± 4.9	45.0 ± 5.3	-
	Area 2	28.3 ± 2.2	66.0 ± 2.15	2.0 ± 0.3	3.7 ± 0.7	-

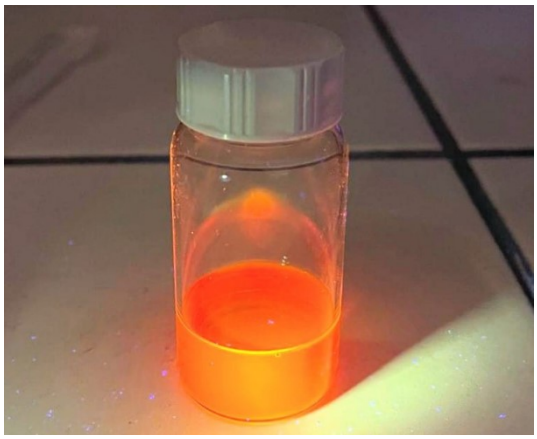

Figure S32: Digital picture of a CIZS@CIT-GSH sample under UV-light irradiation